Materials Letters 284 (2021) 128990

Contents lists available at ScienceDirect

Materials Letters

journal homepage: www.elsevier.com/locate/mlblue

Ultrasonic-assisted preparation of reduced graphene oxide-hydroxyapatite nanocomposite for bone remodeling

Bing Li [a], Bahman Nasiri-Tabrizi [b,*], Saeid Baradaran [c], Chai Hong Yeong [d], Wan Jefrey Basirun [c]

[a] Department of Orthopedic, Xi'an No. 3 Hospital, No. 10, East Section of Fengcheng 3rd Road, Weiyang District, Xi'an, Shaanxi Province 710018, China
[b] School of Biosciences, Faculty of Health and Medical Sciences, Taylor's University, Subang Jaya, Malaysia
[c] Department of Chemistry, Faculty of Science, University of Malaya, 50603 Kuala Lumpur, Malaysia
[d] School of Medicine, Faculty of Health and Medical Sciences, Taylor's University, Subang Jaya, Malaysia

ARTICLE INFO

Article history:
Received 28 August 2020
Received in revised form 28 October 2020
Accepted 5 November 2020
Available online 10 November 2020

Keywords:
Nanocomposites
X-ray techniques
Raman
Microstructure
Carbon materials

ABSTRACT

An ultrasonic-assisted preparation strategy was employed to synthesize *in-situ* hydroxyapatite-reduced graphene oxide nanocomposite (n-HA/rGO) as a potential biomaterial for bone regeneration under the osteoporotic condition. The results of Rietveld refinement indicated that the optimum crystallite size was 20.26 ± 0.52 nm following the ultrasonication at 400 W for 10 min. Well-dispersed plate-shaped HA nanocrystals with the mean thickness of 25 ± 2 nm were formed on the surface of rGO due to its anchoring tendency with calcium ions and hydrogen phosphate. By increasing the amount of power to 500 W, the intensity ratio of the D and G bands (I_D/I_G) increased due to the rise in the perturbation level in the rGO matrix and the chemical interactions between the rGO and HA.

1. Introduction

Osteoporosis, as a global health concern, is a skeletal disorder characterized by low bone mass, which results in increased susceptibility of fractures [1]. Accordingly, various regenerative medicine strategies, including hydrogel therapy, allografts, as well as immunotherapy, have received much attention for the healing of bone disorders [2,3]. In this context, new generations of synthetic biomaterials are being developed as bone grafts due to their large surface area, superior mechanical behavior, and tunable surface functionalities [4]. Among them, carbon materials reinforced HA composites (e.g., graphene/HA, GO/HA, and rGO/HA) emerged as valid candidates not only for filling bone defects in osteoporosis but also as valuable materials in non-medical applications [5,6].

The development of nanocomposites with the ability to regenerate bone is an innovative strategy, wherein the *in-situ* formation and distribution of the reinforcement through wet-chemistry methods and dry approaches are still some major challenges ahead for the further development in orthopedic applications [7]. Therefore, in the present letter, we propose a scheme based on ultrasonication, in which quick *in-situ* formation and decoration of rGO (obtained from GO through a reduction process) with plate-shaped HA are achieved for the first time by optimizing the parameters involved.

2. Materials and methods

Herein, the graphite flakes and dimethylformamide (DMF, 99.99%) as an organic compound were obtained from Ashbury Inc. and J.T. Baker Company, respectively. $KMnO_4$ (99.9%), H_2SO_4 (98%), H_3PO_4 (98%), HCl (37%), H_2O_2 (30%), and ethylene glycol (EG, 68%) were purchased from Merck, Malaysia. Also, $CaCl_2$ and $NH_4H_2PO_4{\cdot}6H_2O$ were procured from Sigma Aldrich, Malaysia. The preparation of GO was performed based on the modified Hummer's method (see supplementary data 1) [8]. To prepare the nanocomposite, in the first step, 3.33 ml of $CaCl_2$ (0.24 M) was dissolved in EG (3.33 ml) and 2 ml GO solution was injected dropwise into the initial solution and stirred for 120 min. Then 3.33 ml of $NH_4H_2PO_4$ (0.2 M) was charged in 3.33 ml of EG and injected into the solution under continuous stirring to generate a uniform solution and leave it for 15 min. In the third step, 24 ml of DMF was added into the final solution with vigorous stirring to obtain a uniform solution. The solution pH was kept constant at 10 by adding NH_4OH. Ultimately, the solution was sonicated using ultrasonic irradiation (Sonics Vibra-cell VCX 750, USA, 20 kHz) at various powers of 400 and 500 W for 10 to 40 min at room temperature, followed by centrifuging of the precipitates, rinsing with water and alcohol, and aging in a vacuum oven at 100 °C.

* Corresponding author.
E-mail address: b.nasiritabrizi@gmail.com (B. Nasiri-Tabrizi).

https://doi.org/10.1016/j.matlet.2020.128990
0167-577X/

X-ray diffraction (XRD, PANalytical's Empyrean) was used to determine the crystal structure and composition of the nanocomposite using *Cu*-Kα radiation in the range of 2θ = 20°-80°, functioned at 45 kV and 40 mA. The morphological properties were measured by the SEM (CARL ZEISS-AURIGA 60), operated at 1.0 kV. FTIR spectroscopy was conducted using a Perkin Elmer System 2000 (USA) in the 4000–450 cm^{-1} range. Raman spectroscopy was carried out using a Renishaw Invia Raman Microscope, a laser excitation wavelength of 514 nm. TGA was done with a TA Q5000 thermal analyzer at a heating rate of 10 °C min^{-1} from ambient temperature to 1000 °C.

3. Results and discussion

Fig. 1a-f displays the Rietveld refinement plot of n-HA/rGO, where the observed and calculated patterns are in good agreement.

From this figure, the refined XRD pattern of the nanocomposite illustrates the characteristic peaks of the HA hexagonal phase (PDF#01–074-0565). Based on the literature, GO possesses a peak that is positioned roughly at $2\theta = 10^{\circ}$. This peak disappears and a new one materializes around $2\theta = 26^{\circ}$ following GO reduction [9]. This peak is much weaker and broader than the HA (002) peak owing to the amorphous nature of rGO, and thus, the rGO peak in these patterns is covered by the highly intensified HA (002) peak with high crystallinity.

The various R-factors attained from the Rietveld refinements are presented in Table S1 (see supplementary data 2). The measured values show that a good fit has achieved over the full diffraction pattern [10]. The refined crystallite size and density were estimated through Rietveld refinement of the XRD profile, where were found to be in the range of 20.26 ± 0.52 and 25.76 ± 0.78 nm as well as 3.134 and 3.136 gcm^{-3}, respectively. Based on the measured values, the optimum crystallite size was achieved after the ultrasonication

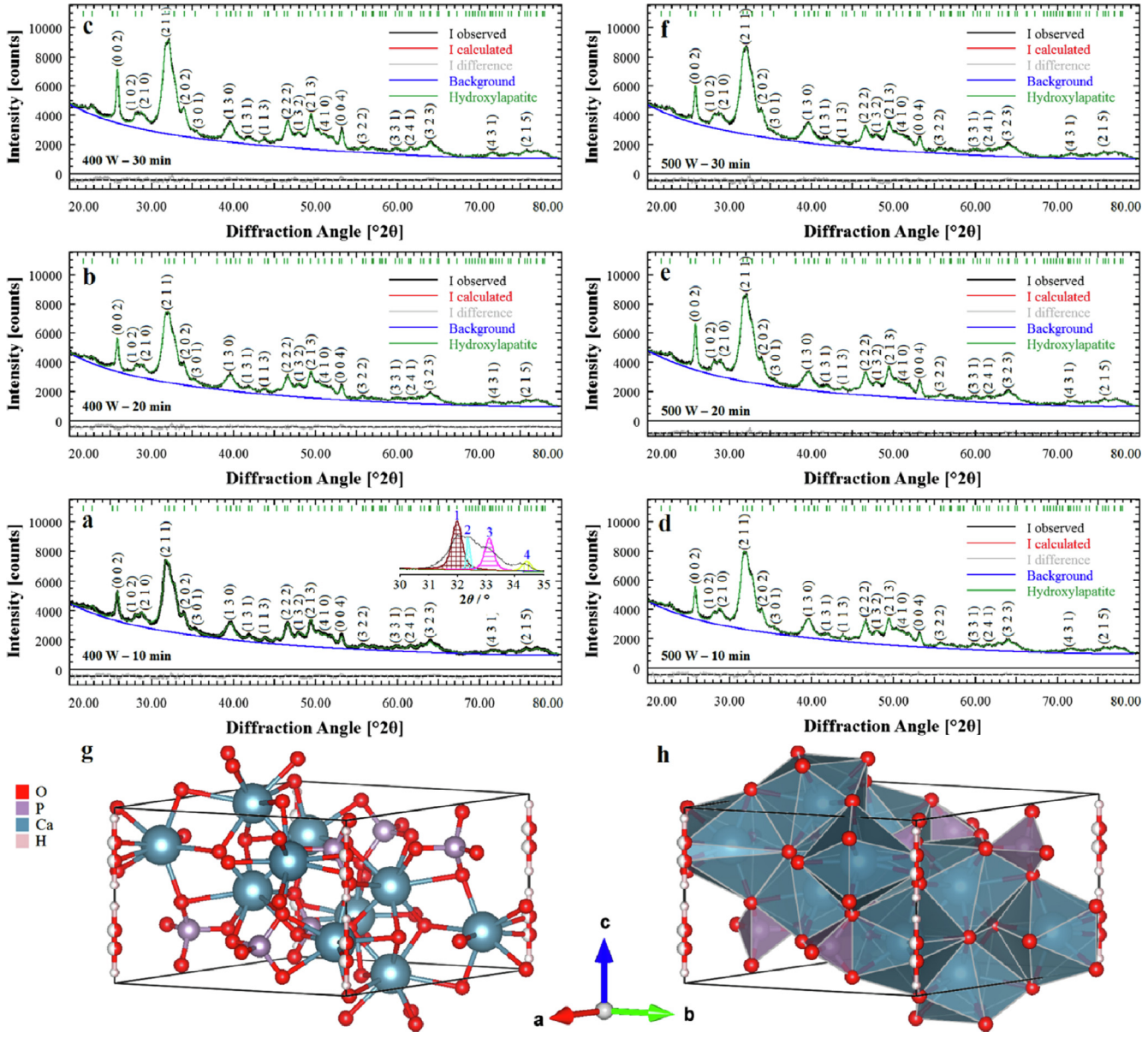

Fig. 1. (a–f) Rietveld refinement plot of n-HA/rGO; (g) ball-and-stick and (h) polyhedral models of the refined structure along with the standard orientation of the crystal shape.

at 400 W for 10 min. In this case, HA has lattice parameters of a = 9.4466 ± 0.0013 Å, c = 6.8846 ± 0.0010 Å, and unit cell volume (V) of 532.0621 Å^3 following the refined models in Fig. 1g and h.

As illustrated in Fig. 2a and b, the two typical GO peaks corresponding to the D and G bands are detected at 1349 and 1607 cm^{-1}. In all cases, the occurrence of the 2D peak at around 2710 cm^{-1} implies a rise in the number of layers in the rGO, where the I_{2D}/I_G ratio remained almost unchanged, indicating that the narrowing of rGO into a few layers of graphene did not occur by increasing the amount of power and time. However, the I_D/I_G ratio increased notably with increasing the power of ultrasonication up to 500 W, denoting the formation of a high concentration of defects and sp^2 bonds in the graphene lattice [11]. From the FTIR spectra in Fig. 2c, the n-HA/rGO exposes all typical bands of rGO (CH_2) and apatitic groups (i.e., PO_4^{3-}, CO_3^{2-}, and OH^-) [9]. Three steps of the weight loss were observed in the TGA curve of the GO, including loss of H_2O molecules in the GO, the thermal decomposition of unbalanced oxygen-comprising functional groups, as well as the carbon skeleton combustion [12]. The n-HA/rGO showed a lower weight loss (~13%) than the GO (Fig. 2d).

It was found that the plate-shaped HA nanocrystals with the mean thickness of 25 ± 2 nm were uniformly decorated on the surface of rGO (Fig. 3a–d). This behavior is caused by the anchoring tendency of rGO with Ca^{2+} and HPO_4^{2-} [7]. From the EDS analysis, Ca, O, and C are the main elements found in the n-HA/rGO with a Ca/P ratio of 1.68. During the *in-situ* decoration of HA on rGO, the oxygen-comprising functional groups on rGO act as recipient places for calcium ions via electrostatic interplays, leading to *in-situ* interacting with the HPO_4^{2-} and forming HA nanocrystals, as shown in Fig. 3e (see supplementary data 3). These findings are consistent with previous studies that demonstrated the ability of n-HA/rGO to quicken bone regeneration [13]. The proposed system

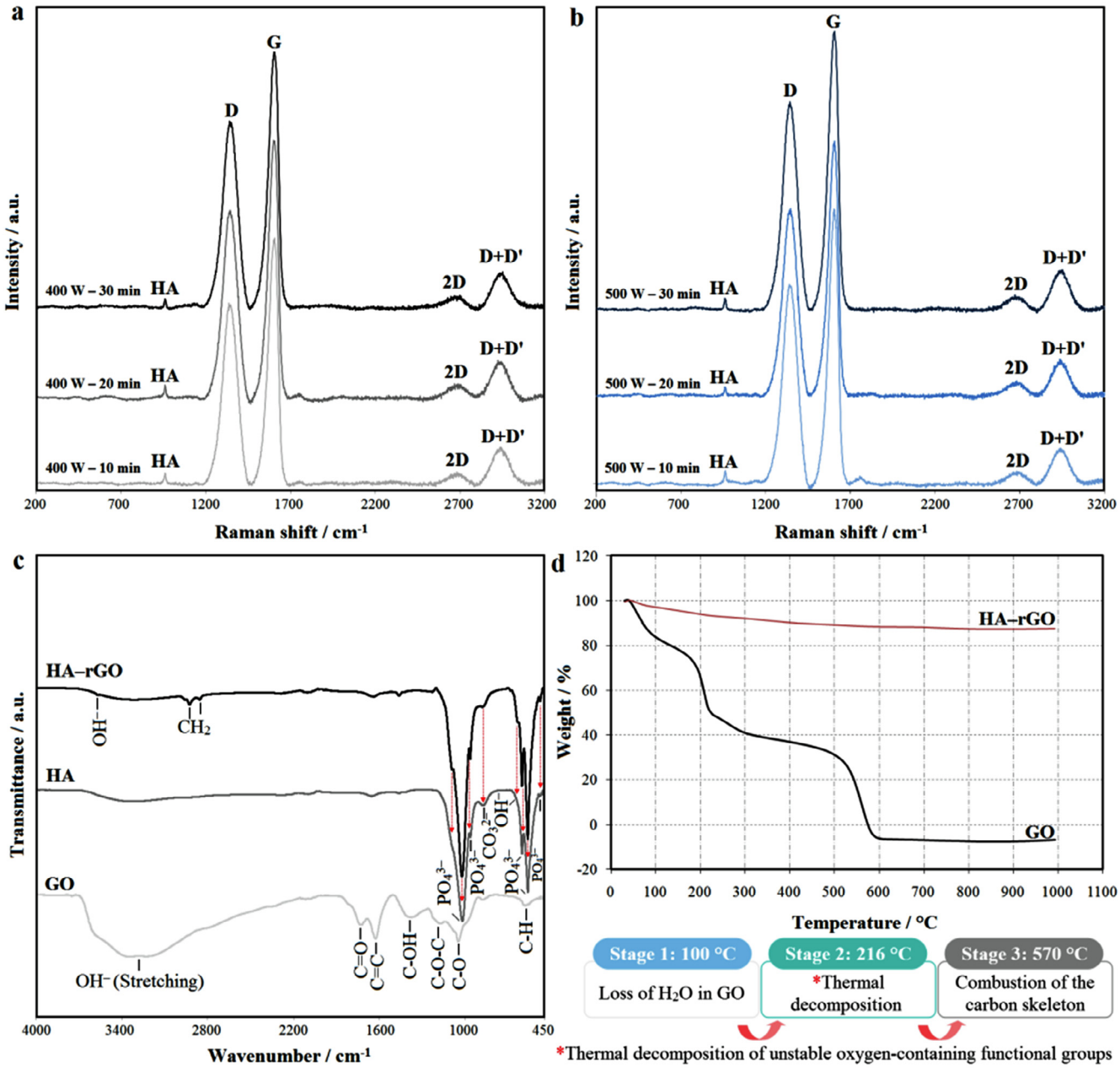

Fig. 2. Chemical structure and thermal stability of n-HA/rGO characterized by (a,b) Raman, (c) FTIR spectra, and (d) TGA.

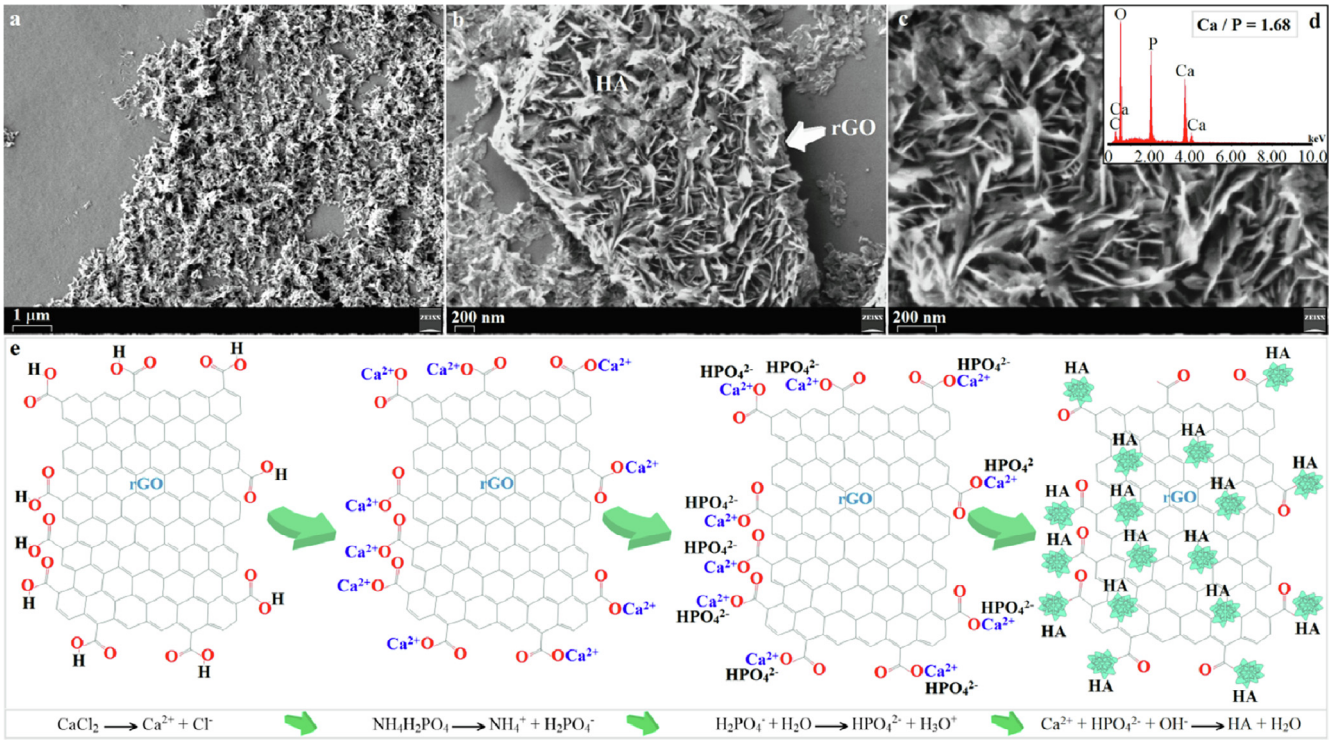

Fig. 3. (a–c) SEM images and (d) EDS spectrum of n-HA/rGO, and (e) the *in-situ* decoration of HA on rGO.

may also be utilized as a selective chemical sensor for the detection of Bisphenol A [14] and as an efficient photocatalyst for tetracycline degradation [15].

4. Conclusions

To conclude, n-HA/rGO was synthesized by the *in-situ* ultrasonic-assisted method. The rGO peak in XRD profiles was covered by the highly intensified HA (002) peak. A good fit by Rietveld refinement was obtained for the nanocomposite, wherein the optimum crystallite size was settled at 400 W for 10 min. From the Raman spectra, the I_{2D}/I_G ratio kept approximately constant, which revealed no occurrence of the thinning of rGO into a few layers of graphene by changing the amount of power and time. The n-HA/rGO exhibited a weight loss of ~13%. A well-decorated structure was observed due to the presence of ion receptors on rGO, which ultimately caused the *in-situ* development of plate-shaped HA on rGO.

CRediT authorship contribution statement

Bing Li: Conceptualization, Investigation, Software. **Bahman Nasiri-Tabrizi:** Methodology, Data curation, Writing - original draft. **Saeid Baradaran:** Visualization, Methodology. **Chai Hong Yeong:** Validation, Supervision. **Wan Jefrey Basirun:** Validation.

Declaration of Competing Interest

The authors declare that they have no known competing financial interests or personal relationships that could have appeared to influence the work reported in this paper.

Appendix A. Supplementary data

Supplementary data to this article can be found online at https://doi.org/10.1016/j.matlet.2020.128990.

References

[1] G.G. Teng, Mortality and osteoporotic fractures: is the link causal, and is it modifiable?, Clin. Exp. Rheumatol. 26 (2008) S125–S137.
[2] M.R. Iaquinta, E. Mazzoni, M. Manfrini, A. D'Agostino, L. Trevisiol, R. Nocini, L. Trombelli, G. Barbanti-Brodano, F. Martini, M. Tognon, Innovative biomaterials for bone regrowth, Int. J. Mol. Sci. 20 (2019) 618.
[3] Y. Chang, B. Cho, S. Kim, J. Kim, Direct conversion of fibroblasts to osteoblasts as a novel strategy for bone regeneration in elderly individuals, Exp. Mol. Med. 51 (2019) 1–8.
[4] Z. Peng, T. Zhao, Y. Zhou, S. Li, J. Li, R.M. Leblanc, Bone tissue engineering via carbon-based nanomaterials, Adv. Healthcare Mater. 9 (2020) 1901495.
[5] F. Peng, D. Zhang, D. Wang, L. Liu, Y. Zhang, X. Liu, Enhanced corrosion resistance and biocompatibility of magnesium alloy by hydroxyapatite/graphene oxide bilayer coating, Mater. Lett. 264 (2020) 127322.
[6] H. Porwal, S. Grasso, M. Reece, Review of graphene–ceramic matrix composites, Adv. Appl. Ceram. 112 (2013) 443–454.
[7] M. Li, P. Xiong, F. Yan, S. Li, C. Ren, Z. Yin, A. Li, H. Li, X. Ji, Y. Zheng, Y. Cheng, An overview of graphene-based hydroxyapatite composites for orthopedic applications, Bioact. Mater. 3 (2018) 1–18.
[8] H. Lim, N. Huang, S. Lim, I. Harrison, C. Chia, Fabrication and characterization of graphene hydrogel via hydrothermal approach as a scaffold for preliminary study of cell growth, Int. J. Nanomed. 6 (2011) 1817–1823.
[9] H. Nosrati, R. Sarraf-Mamoory, D.Q.S. Le, R. Zolfaghari Emameh, M. Canillas Perez, C.E. Bünger, Improving the mechanical behavior of reduced graphene oxide/hydroxyapatite nanocomposites using gas injection into powders synthesis autoclave, Sci. Rep. 10 (2020) 8552.
[10] N. Doebelin, R. Kleeberg, Profex: a graphical user interface for the Rietveld refinement program BGMN, J. Appl. Crystallogr. 48 (2015) 1573–1580.
[11] S. Baradaran, E. Moghaddam, W.J. Basirun, M. Mehrali, M. Sookhakian, M. Hamdi, M.R.N. Moghaddam, Y. Alias, Mechanical properties and biomedical applications of a nanotube hydroxyapatite-reduced graphene oxide composite, Carbon 69 (2014) 32–45.
[12] M. Raucci, D. Giugliano, A. Longo, S. Zeppetelli, G. Carotenuto, L. Ambrosio, Comparative facile methods for preparing graphene oxide–hydroxyapatite for bone tissue engineering, J. Tissue Eng. Regen Med. 11 (2017) 2204–2216.
[13] J.H. Lee, Y.C. Shin, S.-M. Lee, O.S. Jin, S.H. Kang, S.W. Hong, C.-M. Jeong, J.B. Huh, D.-W. Han, Enhanced osteogenesis by reduced graphene oxide/hydroxyapatite nanocomposites, Sci. Rep. 5 (1) (2015).
[14] M.K. Alam, M.M. Rahman, A. Elzwawy, S.R. Torati, M.S. Islam, M. Todo, A.M. Asiri, D. Kim, C. Kim, Highly sensitive and selective detection of Bis-phenol A based on hydroxyapatite decorated reduced graphene oxide nanocomposites, Electrochim. Acta 241 (2017) 353–361.
[15] R. Zou, T. Xu, X. Lei, Q. Wu, S. Xue, Novel design of porous hollow hydroxyapatite microspheres decorated by reduced graphene oxides with superior photocatalytic performance for tetracycline removal, Solid State Sci. 99 (2020) 106067.